Chapter 1

Interpreting seismic monitor data

1.1 Overview

In this chapter, I present an integrated interpretation of six time-lapse 3-D data sets recorded over a steamflood site in the heavy-oil Duri Field, Sumatra, Indonesia. Migrated 3-D images and velocity analysis illuminate fluid-flow features of the steamflood in time-lapse mode. The steam front is visible seismically as large reflection and diffraction responses, and velocity decreases of up to 40%, in a disk centered at the steam injection well. The steam front intensifies in place at a radius of less than 50 m for the first nine months of injection, and then breaks out and rapidly propagates to the northwest of the injection pattern at and beyond the 13-month survey. The steam movement mapped by time-lapse seismic correlates with two temperature observation wells and oil production data from the surrounding producing wells. A thin annulus of hot water (steam condensate) is visible in time slices as a 10% increase in velocity. A transient pressure front is observed at 2 months of steam injection to propagate towards the northwest, but not toward the southeast. Mapping the early pressure front movement predicts where thermal and steam fronts will follow high permeability flowpaths. The steam front is shown to follow the leading pressure front to the northwest one full year after the pressure front was initially mapped. [1]

1.2 Introduction

The steamflood process is a common method of enhanced oil recovery in viscous oil reservoirs. Unfortunately, steam flow directions, rates and sweep efficiency can be unpredictable in the presence of reservoir heterogeneity. These uncertainties can lead to large bypassed regions of unproduced oil, and expensive changes in injection/production well placement, intervals of perforation, and surface steam facility

[1] A modified version of this chapter was presented by Lumley (?) at the Annual International SEG Conference, Houston, TX.

planning. Seismic monitoring may prove to be a valuable tool for optimizing reservoir production strategies in the presence of fluid-flow uncertainty.

1.2.1 Petrophysical basis

Spatial and temporal changes in pore pressure, temperature and fluid saturation in a reservoir during steam injection can cause dramatic changes in reservoir rock properties, e.g., Ito et al. (?), Wang and Nur (?). Time-dependent rock properties during steamflooding can cause seismic wavefields to be distorted and scattered throughout affected regions of the reservoir, compared to unaffected regions. For example, large seismic impedance contrasts associated with steam zones can cause seismic reflections and diffractions, which can be used to image the expanding steam front. Additionally, large seismic velocity decreases associated with heated reservoir rock may be used to map the spatial progress of thermal fronts. In principle, detecting and measuring changes in the seismic response as a function of space and time can lead to a clearer picture of the manner in which steam injection is affecting fluid flow and physical states in the reservoir, and therefore may help to optimize the reservoir production strategy.

1.2.2 Related work

Although the concept of time-lapse seismic reservoir monitoring is relatively new, a few notable pilot projects have been attempted at steam injection sites. Pullin et al. (?) collected two 3-D seismic surveys before and after a steam pilot at an Athabasca tar sands reservoir site. By comparing time delay and amplitude attenuation maps between the two stacked surveys, they were able to qualitatively map the location of heated versus unheated zones. Eastwood et al. (?) performed a similar analysis on a 3-D seismic monitor of an Alberta cyclic steam stimulation (CSS) project. They used two 3-D seismic surveys recorded at separate production and injection cycles, integrated with crosswell data, thermal reservoir simulations, and rock physics measurements. They were able to explain the magnitude of observed traveltime changes between two surveys, but less so the spatial distribution of changes. Non-steam seismic monitoring projects of interest include an in-situ combustion study by Greaves and Fulp (?), and a gascap monitoring study in the Oseberg field by Johnstad et al. (?).

1.2.3 The Duri experiment

A 4-D seismic monitoring experiment has been conducted by CalTex to monitor a steamflood in a viscous oil reservoir in the Duri Field, Sumatra, Indonesia. Multiple 3-D seismic surveys were recorded over a 7-spot steam injection pattern during a period of two years. Two baseline surveys were acquired before steam injection to test experimental repeatability. Five monitor surveys were recorded at an average 4

month interval, ranging from 2 to 19 months after steam injection was initiated. Two temperature observation wells are available, and six core samples were taken from the injector borehole before steam injection at various levels of the reservoir zone.

1.2.4 Current research

An excellent overview of the experiment and first interpretation of the field data was presented by Bee et al. (?). My collaborative role in their paper was to help provide the basic physical links between first-order observed seismic changes, steamflood fluid flow, and rock physics. In this chapter, I delve deeper into this 4-D data set to improve understanding of the complex seismic changes observed between the repeated 3-D surveys in terms of changing reservoir conditions and fluid flow. In particular, I attempt to explain the complex seismic monitor phenomena by integrating a simple model of steamflood fluid-flow with rock physics measurements, finite-difference seismogram modeling, 3-D seismic imaging and velocity analysis.

1.3 Duri Field description

1.3.1 Oil production

Bee et al. (?) give a review of the Duri Field's history and production, and describe the 4-D experiment and initial interpretation. The Duri Field contains 5.3 billion barrels (bbls) of original oil in place (OOIP). Primary production was expected to produce only about 400 million bbls, or about 8% of OOIP, because the Duri oils are very viscous (API gravity is 22°). With steamflooding, about 60% of OOIP is expected to be recovered, representing an additional 2.7 billion bbls of oil over primary production.

Currently, about 40% of the field is undergoing steamflooding. The first steamflood patterns were drilled in 1985 and have increased the field production from about 40,000 barrels per day (BPD) to currently over 350,000 BPD. Over $1.2 billion has been invested in steamflooding to date, and the project is expected to expand to completion for another 25 years. If seismic monitoring can increase production by only 1% of OOIP, an extra 53 million bbls of oil will be gained. Therefore, the incentive for attempting to use time-lapse seismic data to enhance reservoir management is very favorable at this site.

1.3.2 Steam injection

Figure 1.1 shows a diagram of a single "7-spot" steam injection well pattern. The surface area of the 4-D seismic coverage is outlined by the outer box, and is 355 m on a side. The 7-spot is composed of six producing wells (black circles) connected in a hexagon, with the seventh well being the steam injector in the center (open circle with

arrow). Additionally, two temperature observation wells (open circles) are located on either side of the injector.

Steam is being injected into two reservoir zones, as shown in Figure 1.2. Each zone is separated by thermal packers. The upper steam zone is in the P formation, which ranges from 140–200 m depth, or 155–210 ms in seismic traveltime. The lower steam zone is in the K formation, which ranges from 200–230 m in depth, or 210–245 ms in seismic traveltime.

Clay layers are suspected to cause flow barriers in the reservoirs, and heterogeneity can make steam flow directions unpredictable. For these reasons, a pilot 4-D seismic monitor experiment was conducted over this small steam injection pattern to see if vertical and lateral steam flow could be mapped from time-lapse seismic monitor data.

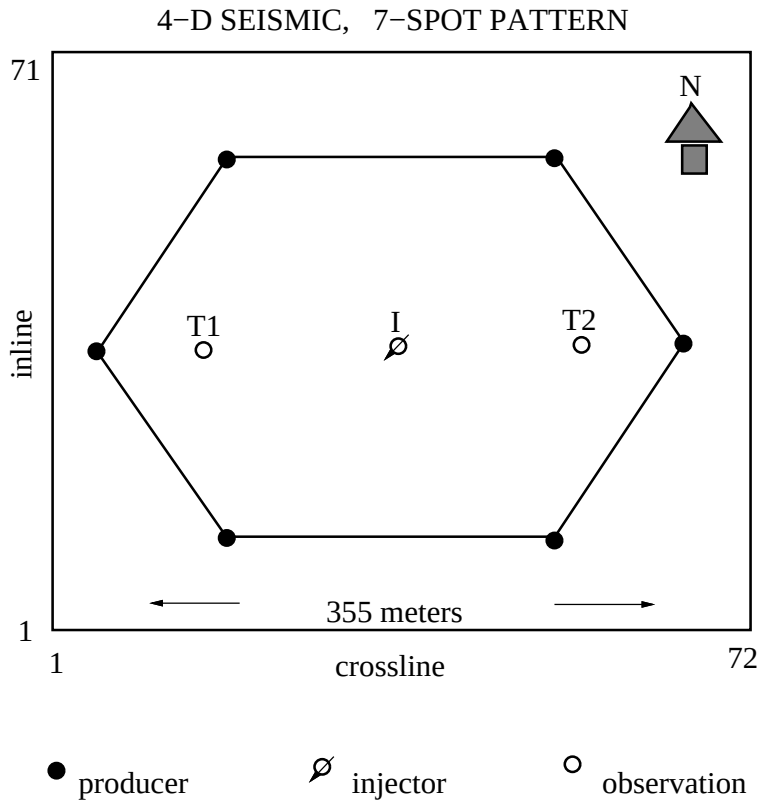

Figure 1.1: Duri 4-D seismic coverage over a 7-spot steamflood pattern. The steam injection well is at the center, flanked by two temperature monitor wells on either side. interp-7-spot [NR]

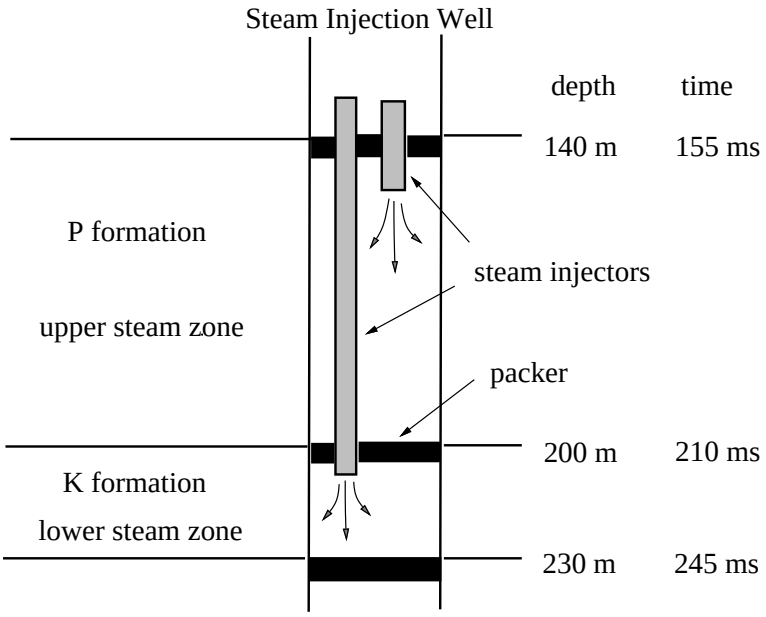

Figure 1.2: Steam injection zones at the injector well (after Bee et al., 1994). interp-zones [NR]

1.4 Seismic acquisition

1.4.1 Time-lapse schedule

A total of seven 3-D seismic data sets have been acquired over the injector pattern of Figure 1.1. The timeline of the seismic surveys is shown in Table 1.1 with respect to the start of steam injection. Two baseline surveys were collected 3 days apart prior to steam injection in July 1992 for comparison with surveys taken during steam injection. The repeatability of the seismic measurements was confirmed with two baseline surveys to ensure that changes in repeated 3-D surveys were due to subsurface conditions, not acquisition-related variations. Continuous steam injection started in August 1992 and continues at the present time. Five 3-D seismic monitor surveys were acquired at intervals of 2, 5, 9, 13, and 19 months after the start of steam injection.

1.4.2 Survey geometry

Each 3-D survey consists of 301 shots fired into a fixed array of 480 receivers, as described in Figure 1.3 and Chapter 4. Each shotpoint consists of a small dynamite charge (50 g) fired in a shot hole at 15 m depth. Each receiver is a single hydrophone immersed in water at 7 m depth. Frequencies in the data exceed 200 Hz at a 1 ms sample interval. The maximum offset in the data is 480 m, with a good range of offset and azimuthal coverage. Maximum fold is 80 in the center of the pattern, and 24 at

DATE	EVENT	ELAPSED TIME
July 1992	baseline survey	-1 month
August 1992	start steam injection	0 months
October 1992	monitor 1 survey	2 months
January 1993	monitor 2 survey	5 months
May 1993	monitor 3 survey	9 months
September 1993	monitor 4 survey	13 months
March 1994	monitor 5 survey	19 months

Table 1.1: Timeline for steam injection and time-lapse seismic surveys.

the edges of the hexagon of producing wells. Figure 1.4 shows the CMP bin centers for each 3-D survey, and Figure 1.5 shows the spatially variable CMP fold coverage. A complete 3-D survey can be acquired in one working day.

Figure 1.3: Overlain shot and receiver locations of the 4-D monitor survey. Shots are marked "x", and receivers are marked "o". interp-survey [ER]

Figure 1.4: CMP bin-center locations of the 4-D monitor survey. interp-bins [ER]

1.5 Seismic images of fluid flow

I did extensive data processing of the Duri 4-D seismic data, as described in Chapter 4. In this section, I present a few examples of the data results in order to motivate the detailed integrated interpretation that follows. A complete set of time-lapse images will accompany the final interpretation.

Figure 1.6 shows 3-D stacked inline sections of the baseline, monitor 2 and the difference between the two. Figure 1.7 shows the same display of the 3-D migrated inline data. The location of the inline sections passes through the two temperature observation wells and the steam injector, as shown in Figure 1.1. Steam has been injected continuously for five months at the time of these monitor 2 images.

1.5.1 Repeatability

Both the inline stacks and migrations show that the data above the reservoir (less than 150 ms) is highly repeatable. This is especially apparent by noticing that the overburden contains mostly incoherent noise in the stacked and migrated difference sections. Repeatability in the overburden is important in order to ensure that any changes seen in deeper portions of the time-lapse images are truly associated with fluid flow in the reservoir.

Figure 1.5: CMP spatially-variable fold of the 4-D monitor survey. interp-fold [ER]

1.5.2 Steam leak

A notable exception to the repeatable nature of the overburden is the thin anomaly in the migration difference section at the center of the profile, labeled "B" at about 750 ms pseudodepth. This anomaly may be the effect of a steam leak in the shallow portion of the injection well. The subsequent heating and desaturation around the borehole region would be likely to cause such a narrow vertical band of time delay in the center of the profile. Later migration profiles show this region to extend vertically with calendar time.

1.5.3 Steam zone diffractions

Three sets of large amplitude diffractions are visible in the stacked sections of Figure 1.6, labeled "D1–D3". The D2 diffraction appears to have the strongest amplitude. Its location at 200 ms depth corresponds almost exactly with base of the upper steam zone in the P formation (Figure 1.2). The D1 and D3 diffractions are weaker than the D1 diffraction, and correspond to the top of the P formation (165 ms) and base of the K steam zone (240 ms) respectively. These diffractions are probably due to the concentrated zones of steam, as will be demonstrated in the seismic modeling and interpretation section of this paper.

1.5.4 Polarity changes and vanishing reflectors

The time-lapse seismic images show some dramatic changes in amplitudes along baseline reflectors. Strong reflectivity changes are visible in the monitor 2 survey, compared to the baseline survey, along the reflector at the base of the P formation (200 ms). In the monitor 2 images, at the west (left) side of the injector, the baseline reflection has almost completely vanished out to the survey edge. This feature is labeled "Z" in the stacked and migrated images of Figures 1.6 and 1.7, and indicates that an impedance match has occurred across the P/K formation boundary, perhaps by differential heating from above and below, or pressure changes in the P formation alone. On the other side of injector, towards the east (right) the monitor 2 sections show what appears to be a polarity reversal along the P/K formation boundary at 200 ms, labeled "Pr". This feature is also clearly evident in both the stacked and migrated difference sections, and may be explained by a thin gravity override steam zone traveling along the upper portion of the K reservoir to the east, but not the west.

1.5.5 Imaged steam zones

In the migrated difference section, and to a lesser extent in the stacked difference section, some seismic features are visible that correlate with the known intervals of steam injection. In the migration difference section, a crisp image of a steam zone reflection is visible at about 165 ms depth (labeled "S1"), which is near the top of the upper steam zone in the P formation. A fairly strong steam zone reflection (S2) is imaged at the base of the P formation (210 ms), and a much weaker response (S3) correlates with the base of the K formation (245 ms). These steam zone reflections are obtained by migrating the diffraction responses D1–D3, and are likely to be direct evidence of steam accumulation.

1.5.6 Time pull-up and delay

The migrated images show considerable time delay in the vicinity of the injector, especially near the S2 zone at the base of the P formation. These time delays are likely to be caused by a velocity decrease in the reservoir due to heating and replacement of pore fluid with steam. Additionally, some evidence exists for time pull-up (reflection events which arrive at smaller traveltimes due to velocity increase) to the west of the injector. I will later discuss how these time pull-ups may be caused by velocity increases associated with a pressure front that has propagated to the west.

1.5.7 Spatial images of fluid flow

Figure 1.8 shows a 3-D migration time slice before and after steam injection, at a pseudodepth of 208 ms, which is right at the base of the P reservoir (upper steam zone), and just above the top of the K reservoir (lower steam zone), as shown in Figure 1.2. The inline sections described above pass through Figure 1.8 from west to east through the center of the time-slice image. Comparing time slices before and after steam injection, some obvious seismic anomalies are visible around the injector location.

The bright white disk labeled "S" is almost certainly steam, not just heated fluid, as will be explained in later sections of this paper. The dark annulus to the east labeled "Pr" is the polarity reversal along the east base of the P formation, as observed in the inline sections. However, the time slice shows that the polarity reversal actually forms a semi-circular annulus around the well on the east and south side. On the west, the region where the base of the P formation apparently vanished is labeled "Z". I will later explain why I think that a pressure front has already propagated out of the picture to the northwest, leaving behind an impedance match that causes the base P reflector to vanish to the west. Finally, a thin dark annulus is visible in the time slice very close to the injector, labeled "W". I believe this may be the seismic image of a thin ring of hot water that is created by steam condensing in the reservoir close to the injector.

1.5.8 Seismic questions

I have described some very complex and intriguing features visible in the time-lapse seismic images. These features are almost certainly associated with fluid-flow processes in the P and K reservoirs since they correlate with steam injection depths, and very few seismic changes are seen in the overburden images. Similar features are visible in the other time-lapse data sets, and evolve spatially with time. Such dramatic changes in seismic data during steam injection raise many interesting questions, including the following:

- Do the bright reflections and time delay in the reservoir indicate the presence of steam, or merely heated regions?
- Should we be able to distinguish separate fluid-fronts of water, oil and steam?
- Can we resolve the vertical and lateral distribution of steam in the upper and lower formations?
- What could be causing time pull-up (velocity increase) to the north and west of the injector?
- What is the explanation for the large polarity reversal to the south and east along the base of reservoir reflection?
- Why are changes within the reservoir confined to a radius of only 50 m, whereas changes below the reservoir extend at least 350 m out to the edge of the survey area?

In the following sections, I attempt to answer some of these questions by carefully considering a simple model of steamflood fluid flow, rock physics core measurements and analysis, finite-difference seismic modeling, and seismic image and velocity analysis.

Figure 1.6: 3-D stacked inline sections: before steam injection (left), after 5 months of steam (center), and the difference (right). interp-inline-stks-ann [ER]

Figure 1.7: 3-D migrated inline sections: before steam injection (left), after 5 months of steam (center), and the difference (right). interp-inline-migs-ann [ER]

Figure 1.8: 3-D migrated time slices at the base of the P reservoir (208 ms): before steam injection (top), and after 5 months of steam injection (bottom). interp-tslice-migs-ann [ER]

1.6 Reservoir fluid-flow physics

In this section, I propose a highly idealized model of steamflood. Combining the simple physical features of the steamflood model with reservoir properties, core measurements and rock physics analysis, I am able to make some predictions about the nature of anticipated seismic responses during the steamflood process.

1.6.1 Reservoir properties

The two reservoir zones undergoing steamflood are located at a depth of 140–230 m (155–245 ms), as depicted in Figure 1.2. The reservoir matrix is composed of unconsolidated sands, silts and clays. This very unconsolidated material has high porosity values of about 30–38%, and is very permeable at about 1–8 darcies (**?**). In general, the lower portion of the P formation (210 ms) has the best reservoir quality, with only about 5% clay and mica content by weight from core measurements. In contrast, the upper part of the P formation and the K formation have clay contents of about 12–15%, and core samples from these zones tend to have lower porosity and permeability readings.

Duri oils are very viscous with an API gravity of 22°, and viscosities of 100–1000 cp. The initial oil saturation before steam injection ranges from 29–69%, with an estimated initial gas saturation of about 10%. The initial free gas in pore space is a result of pressure depletion to below bubble point during primary oil recovery. Bubble point pressure is estimated to be about 110 psia, and the initial pore pressure in the reservoir is estimated to be just below that at about 100 psia, and as low as 50 psia at the production wells. The overburden pressure at the reservoir is about 530 psia, which means that initial differential pressures on rocks with 100 psia pore pressure are about 430 psia. Ambient reservoir temperature is about 100 °F [2].

1.6.2 Steamflood model

It is convenient to have an idealized model of the steamflood fluid-flow physical properties in order to make some predictions about the nature of rock physics and seismic responses during steam injection. I consider four separate fluid zones associated with a simplified steamflood:

[2]Conversion to Celsius: $C = 5/9(F - 32)$

- a high-pressure, high-temperature desaturated steam zone.
- a high-pressure, high-temperature saturated water zone,
- a high-pressure, high-temperature saturated oil zone,
- a high-pressure, low-temperature saturated oil zone,

This simple model is diagrammed in Figure 1.9.

1.6.3 Gravity override

This model is slightly more complicated than the conventional block model of a steam zone, a hot condensate zone, and a cold oil zone, but does not try to incorporate the complexity of mixed fluid phases, emulsions, fingering, gravity overrides, etc., as described by Lake (**?**) for example. As a point of interest, the seismic images show no evidence of gravity override at the top of the P formation. If a thin steam zone existed along the formation top, it would show up as a bright reflection, and possibly cause some time delay below, depending on its thickness. The reason that gravity override is not visible may be because the permeability and absence of clay is much higher at the base of the P formation than at the top. This would inhibit steam from racing along the top of the formation, and favor it spreading slowly along the base of the unit instead.

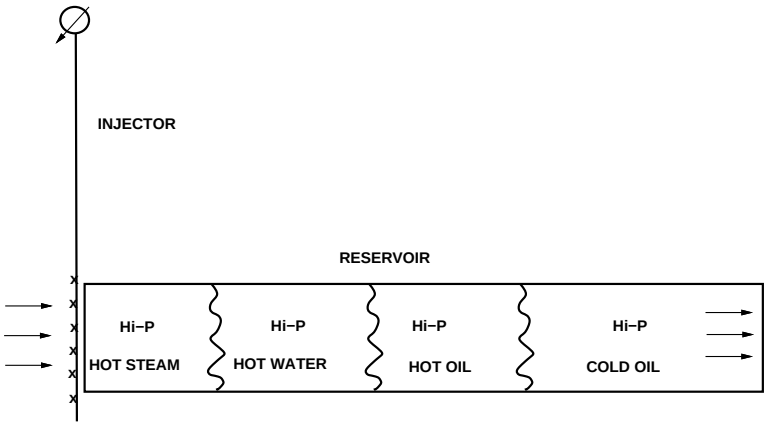

Figure 1.9: An idealized model of steamflood fluid flow. A rapid high-pressure cold front is expected to lead the injector flow, trailed by hot oil, hot water and hot steam zones. The relative dimensions of each zone are not to scale, and complexities such as mixed phases and gravity overrides are neglected. interp-steam-fronts [NR]

1.6.4 Fluid-flow propagation speeds

The simple steamflood model is qualitatively supported by empirical observations. In well-to-well pressure transient tests, it takes on the order of hours to days for a

pressure pulse at one well to propagate to an adjacent well. Pressure is transmitted through the fluid in the connected pore space at a relatively fast rate because it does not require fluid transport to propagate diffusively. Temperature observation wells show that thermal fronts take on the order of weeks to months to propagate similar well-to-well distances. This is because heat transfer occurs through a combination of conduction and convective transport of heated fluids through the permeable pore space, both of which tend to be relatively slow processes. Finally, a desaturated steam zone propagates even slower than a thermal front, because of the additional work required to drive fluid out of pore space. Hence, a steam zone propagates at the speed that heat is conducted through the rock matrix, which is much slower than either convective thermal transport, or pressure diffusion.

To first approximation, according to empirical observations, a steam-induced pressure front should travel at least one order of magnitude faster than the associated thermal or steam fronts. This implies that a distant observer in the reservoir will first notice an increase in pressure but not temperature. The next zone to arrive will be high-pressure heated oil as the thermal effects propagate outward from the steam injector. A hot water zone of condensed steam follows and heats the oil ahead of it. Finally, closest to the injector, a hot steam zone with negligible fluid saturation exists as the heat source that drives the total fluid-flow process.

1.6.5 Pressure, temperature, and saturation changes

Duri engineers estimate that steam is injected into the reservoir at the wellbore at about 430 °F and 350 psia. At the steam front between steam and hot condensate, the pressure and temperature may initially be about 250 psia and 350 °F, and later drop to 135 psia and 350 °F as the steamflood matures (**?**). Residual oil saturation in the steam zone is estimated to be about 10% with gas saturation at 90%. In the hot water and hot oil annulus, temperatures drop off between the steamfront values and ambient reservoir values of 100 °F and 100 psia. Residual oil saturation may be as high as 20%, and gas saturation is probably negligible. In the pressure-front region, pressure values of 110 psia or more will be above bubble point at an ambient temperature 100 °F. Residual gas saturation is likely to be negligible since initial gas in pores space crosses the bubble point and dissolves into liquid oil (path AB of Figure 1.10). The pressure, temperature and gas saturation changes expected in the reservoir during steam injection are tabulated in Table **??** respectively.

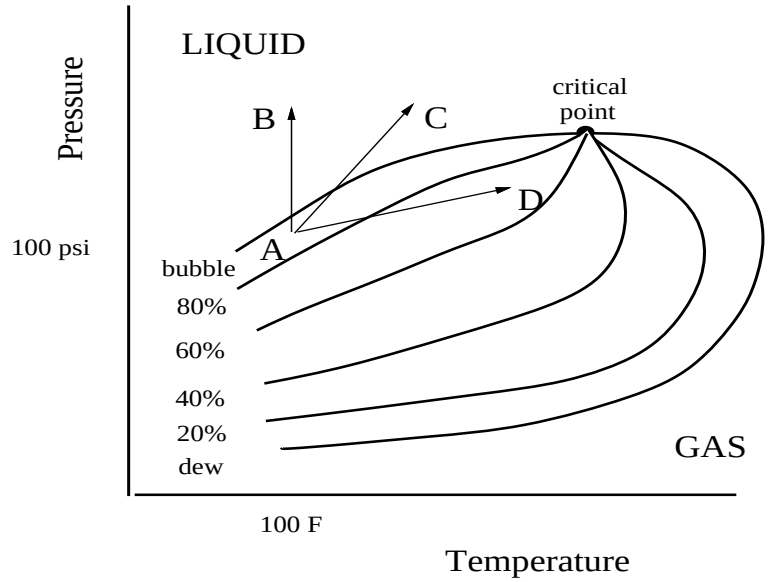

Figure 1.10: Hydrocarbon phase diagram in the Pressure-Temperature plane with contours of liquid oil saturation relative to gas (after Dake, 1978). interp-hc-phase [NR]

1.7 Rock physics

1.7.1 Core measurements

Rock physics core measurements were made at Chevron's core lab facility (?). Six core samples were taken from the injection well location in the P and K formations prior to steamflooding. The samples range from clean fine sand, to clay/silt/sand. The samples show highly unconsolidated sedimentary material. Some samples show coarse sand pockets that might represent potential high-porosity, high-permeability micro channels.

1.7.2 Velocity vs. temperature

The core samples were found to be very sensitive to pressure and temperature conditions. V_p decreases of 10–15% were measured for temperature increases from 75 °F to 250 °F at fixed overburden pressures of 430–600 psia for samples in the upper and lower P formation, and the K formation (Figure 1.11). Above 250 °F, the P-wave velocity decreases a further 25% out to 350 °F since the water component vaporizes to steam.

1.7.3 Velocity vs. pore pressure

At various fixed overburden pressures and temperatures, V_p decreases 3–9% fairly linearly as pore pressure increases from 100 psia to 400 psia in saturated samples. This is due to grain matrix elasticity alone, not to any phase change in the pore fluid.

1.7.4 Velocity vs. gas saturation

Pressure increases can cause the free gas in pore space to dissolve into liquid oil as it crosses the bubble point (Figure 1.10). Wang's measurements on Duri cores suggest that the effect of a decrease in gas saturation from 10% to 0% results in a velocity increase of 19–26%. An increase in gas saturation from 10% to 25% or more results in a 10–15% decrease in velocity. These results are plotted in Figure 1.12.

1.7.5 Density variations

The Duri core measurements show that the density of dry samples ranges from 1.54–1.67 g/cc. Assuming a grain density of 2.67 g/cc, and an average porosity of 35%, a 100% water saturated sample has a density of about 1.95 g/cc and does not vary with temperature. A partially water saturated sample with 10% initial gas saturation has a density of about 1.92 g/cc. The density of Duri oil varies with temperature linearly from 0.92 g/cc at 80 °F to 0.83 g/cc at 350 °F. A sample with 50% oil, 40% water and 10% gas has a density of about 1.90 g/cc at 100 °F, and a density of 1.89 g/cc at 250 °F. A sample with 10% oil and 90% gas (steam) at 350 °F has a density of about 1.63 g/cc. As far as seismic impedance changes are concerned, the only case of interest is that of the steam zone, where density will decrease about 15% compared to initial reservoir conditions. All other scenarios cause negligible density changes, as described above.

1.7.6 Steamflood rock properties

Based on the simple steamflood model of Figure 1.9, and the core measurements taken by Wang and Cates, some rock physics analysis can be made to give approximate estimates of seismic velocity changes that may occur in the reservoir during the steamflood. These rock physics predictions give an indication as to what might be observed in time-lapse 3-D surface seismic monitor surveys. The effects of pressure, temperature, gas/fluid saturation, and the hydrocarbon P-T phase diagram are considered for each of the four steamflood fluid-flow zones described previously.

1.7.7 Steam zone

Table ?? indicates that the steam zone is characterized by a pore pressure increase of about 150 psia, a temperature increase of about 250 °F, and a gas saturation

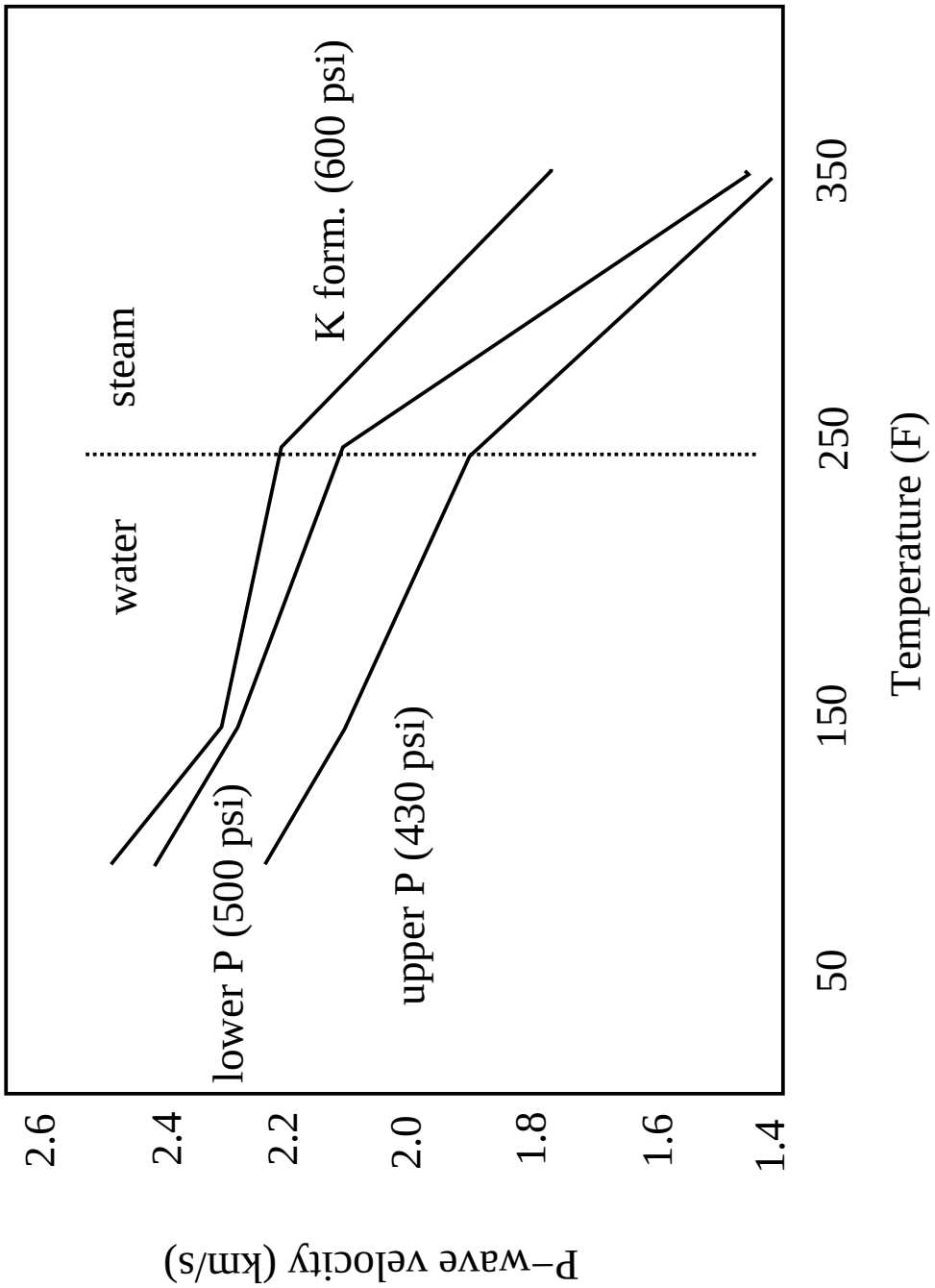

Figure 1.11: P-wave velocity as a function of temperature and overburden pressure for three saturated samples from the upper P, lower P, and K formations (after Wang and Cates, 1994). interp-Vptemp [NR]

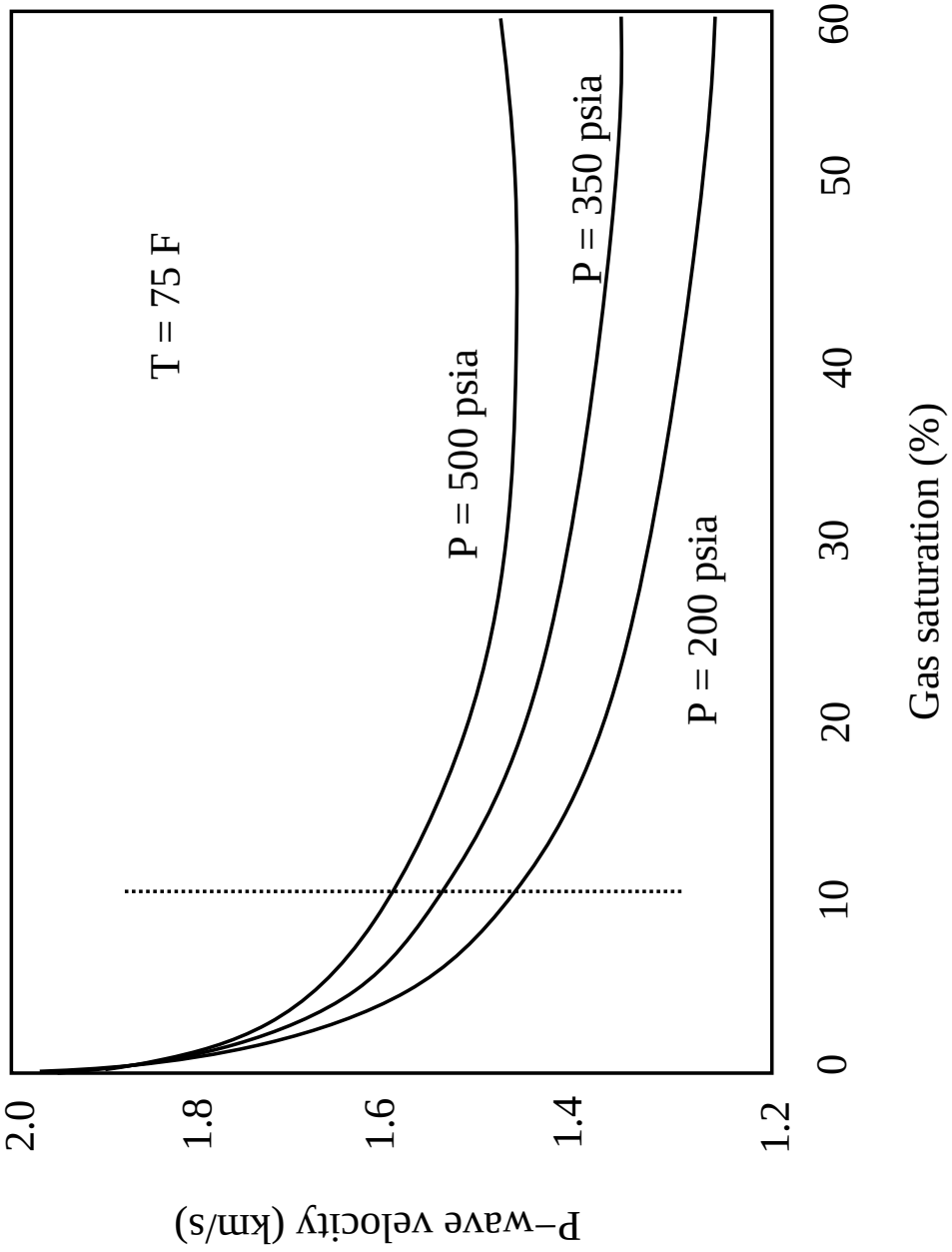

Figure 1.12: P-wave velocity as a function of gas saturation for a saturated sample at differential pressures of 200, 350 and 500 psia (after Wang and Cates, 1994). interp-Vpsg [NR]

value of about 90%, compared to ambient conditions. The pore pressure increase results in a V_p decrease of about 5%. The temperature increase and replacement of water with steam vapor causes a net decrease of about 35–40%, from Figure 1.11. The combined effect of heat, pressure and steam vapor suggests that the steam zone should be associated with a total V_p decrease of 40–45%! Since the gas saturation increases to 90%, the density of rocks in the steam zone should decrease by about 15%. The magnitude of these combined velocity and density changes is very dramatic and should be easily visible in time-lapse seismic data as large time delays and bright reflections and diffractions at the steam zone.

1.7.8 Hot water zone

Table **??** indicates that the hot water zone is characterized by a pore pressure increase of 100 psia, a temperature increase of about 150 °F, and a reduction of gas saturation to about 0%, compared to ambient reservoir conditions. The pore pressure increase results in a V_p decrease of about 5%. The temperature increase of the pure water phase results in a small 5% V_p decrease, from core measurements by Wang and Nur (**?**). The reduction of the gas saturation from an initial 10% to a final 0% may result in a V_p increase as large as 20–25%. Combining these effects implies that the hot water zone may be characterized by a net increase in V_p by 5–10%. Density variations are negligible.

1.7.9 Hot oil zone

Table **??** indicates that the hot oil zone is characterized by a pore pressure increase of about 75 psia, a temperature increase of about 75 °F, and a reduction of gas saturation to about 0%, compared to ambient reservoir conditions. The pore pressure increase results in V_p decrease of 5% at most. The temperature increase in mixed oil/water saturated cores results in a V_p decrease of about 15%, as shown in Figure 1.11. The reduction of the gas saturation from an initial 10% to a final 0% may result in a V_p increase as large as 20–25%. Combining these effects, the net change in velocity at the hot oil zone may be negligible, compared to initial reservoir conditions. Since the density change is also negligible, the hot oil zone may be seismically transparent.

1.7.10 Pressure front

Table **??** shows that the leading pressure front from the injector has a pore pressure increase of at least 50 psia, with no change in temperature. Since the reservoir pore pressure is initially at 100 psia, and the bubble point is estimated to be about 110 psia, large regions of the pressure front could easily be above bubble point. In this case, the initial 10% free gas in pore space would be dissolved into liquid oil. If that happens, a V_p increase on the order of 20–25% could occur. This may be slightly counterbalanced by a 5% decrease in V_p from pore pressure softening of the rock matrix. However,

the net result would be a 20% increase in V_p in regions of the pressure front which are above bubble point. Density variations would be negligible. The combined rock property changes in the pressure front should be seismically apparent by significant time pull-ups and potential reflection polarity changes.

The velocity and density changes in each steamflood zone, compared to the initial reservoir conditions, are summarized in Table **??**.

1.7.11 Steamflood velocity contrast profile

Figure 1.13 shows the predicted velocity contrast profile in the radial direction away from the injector, obtained by combining the rock physics results above. An impedance profile should look similar since density changes are negligible in each zone, except for the steam zone in which the polarity of the contrast is the same as velocity (negative). A rapidly outward-propagating pressure front leads the thermal fronts, and if the reservoir is initially just below the bubble point pressure, the pressure front will appear seismically as an increase in V_p by about 20%, marked by velocity time pull-ups and variable reflection coefficients.

The thermal fronts are likely to lag behind the leading pressure front by many months of steam injection. The outermost thermal front is likely to contain hot oil and be nearly seismically transparent, since it has a negligible velocity contrast. Just behind the hot oil front, a hot water front of condensed steam may exist. It represents a velocity increase of about 10% if the initial 10% gas saturation is reduced to 0%. Finally, a small stable steam zone should surround the injector, perhaps growing in diameter at a very slow rate. This steam zone has a net decrease in V_p of about 40% and should be very visible in the seismic monitor data by strong velocity time delays and very bright reflection coefficients.

1.8 Seismic modeling

Combining the steamflood model and rock physics analysis, I now show some finite-difference seismogram modeling examples to examine what the seismic response to steamflooding might look like. I show simple velocity models of the steamflood, wavefield snapshots, shot gathers, and plane-wave stacks.

1.8.1 Velocity models

Figure 1.14 shows three 1-D velocity profiles. Each one is identical except for the reservoir zone containing either: original cold oil, steam, or the high-pressure front. The velocity model before steam injection is shown in Figure 1.15, and after steam injection in Figure 1.16. Note that after steam injection there is a large low velocity zone near the injector, and a high-velocity high-pressure front propagating in an annulus away from the injector.

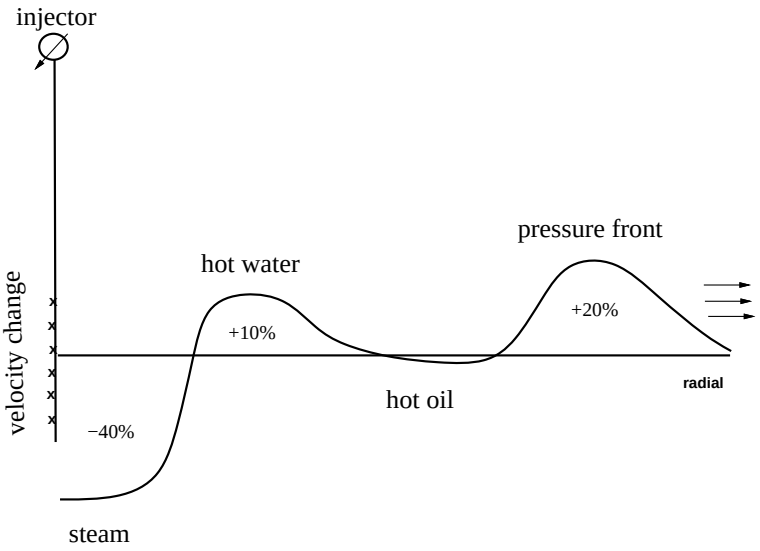

Figure 1.13: Predicted steamflood P-wave velocity contrast profile compared to initial reservoir conditions as a function of radial distance from the injection well. interp-steam-dVp [NR]

1.8.2 Point-source modeling

Using the velocity models of Figures 1.15 and 1.16, I simulated shot gathers by finite difference acoustic modeling. The shot is located at the injector location, and the data are modeled with about 200 Hz maximum frequency content, to match the field data. Figure 1.17 shows a snapshot of the wavefield before and after steam injection. Note that the steam snapshot has a much larger upgoing reflection branch, and is slightly flattened due to time delay on the leading downgoing branch.

Figure 1.18 shows the shot gathers corresponding to the two point-source shots before and after steam injection. Note that the top of reservoir reflection at 210 ms has changed dramatically. It is much brighter and contains both an amplitude zero-crossing and polarity reversal. This occurs where the low-velocity steam zone transitions into the high-velocity pressure front. These amplitude effects might explain the impedance match seen in the field data of Figures 1.6 and 1.7, and suggest that there is a pressure front in the field data. The polarity reversal might be explained by a thin zone of decreased V_p associated with a thin steam gravity override at the top of the K formation. Finally, note the modeled diffractions emanating from the steam zone. These qualitatively match diffractions seen in the field data, and suggest the lateral extent of the steam zone.

1.8.3 Plane-wave modeling

Figure 1.19 shows a finite difference acoustic simulation of a plane wave source leaving the surface at vertical incidence. The snapshot shows that the plane-wave is delayed by the steam zone in the center at the injection well, compared to the pre-steam

synthetic. Diffractions are clearly visible at the center point. The outer limbs of the plane wave are pulled up in time, but the effect is too small to see in a static display.

Figure 1.20 shows the "wave-stack" (**?**) that would have been recorded at the surface for the vertically incident plane-wave source. This wave-stack is similar to an NMO stack section, except it makes no velocity assumption. Note the presence of a strong diffraction associated with the steam zone. Also note the polarity changes and zero crossing along the top reservoir reflection from the steam zone to the high-pressure zone. The wave-stack clearly shows velocity time delay and amplitude focusing below the steam zone, and time pull-up at the survey edges beneath the portion of the reservoir containing the high-pressure front. All of these effects are somewhat visible in the field data sections of Figures 1.6 and 1.7.

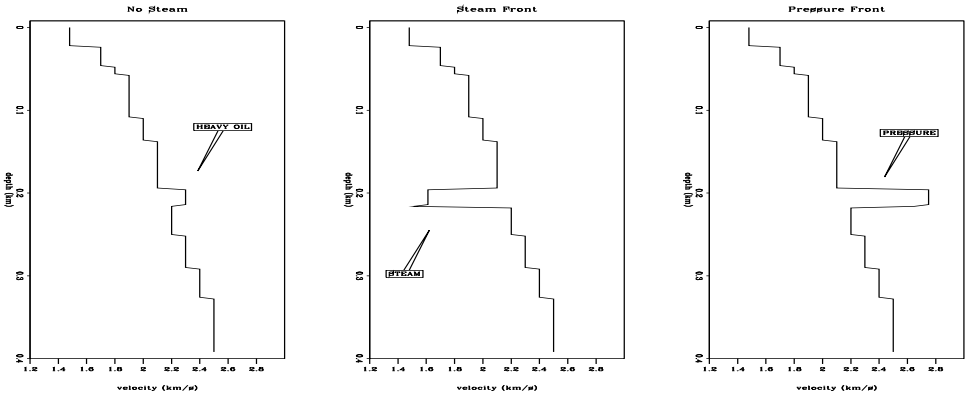

Figure 1.14: Velocity profiles of reservoir containing: viscous oil (left), steam (center), and high-pressure dissolved gas (right). interp-vp123g-ann [ER]

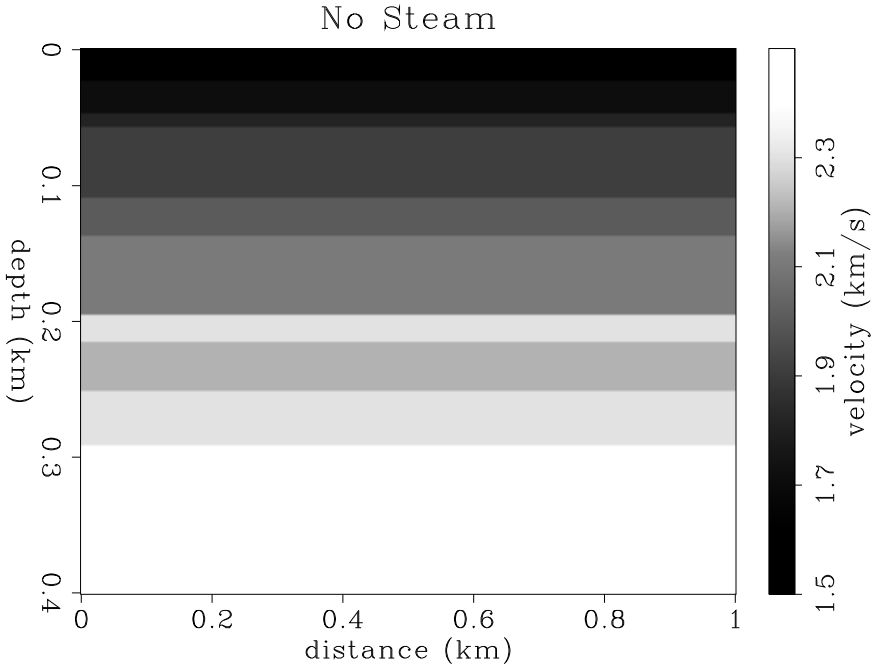

Figure 1.15: Velocity model before steam injection. Heavy-oil reservoir is at 200 m depth. interp-vp1 [ER]

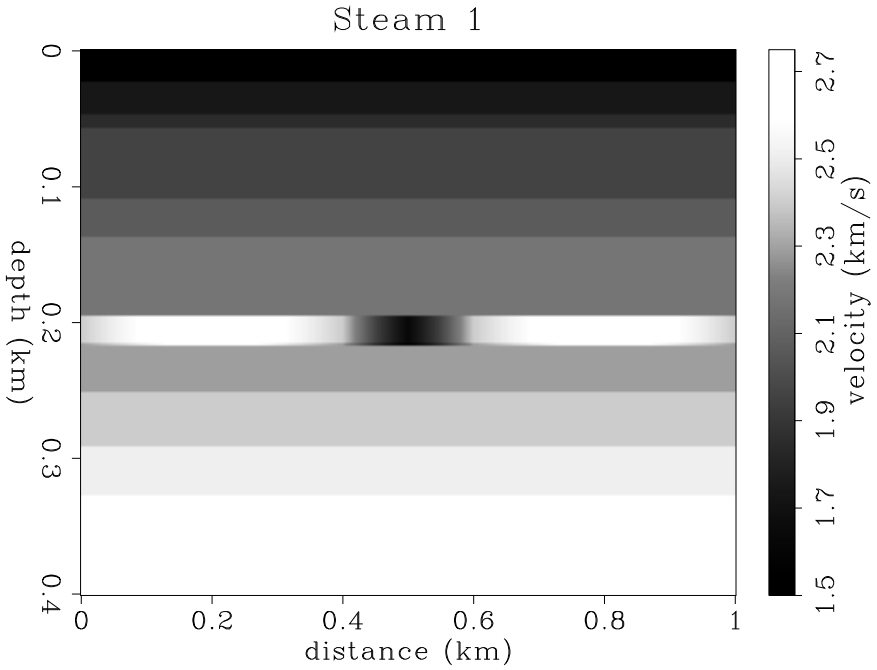

Figure 1.16: Velocity model after 5 months of steam injection. Low velocity anomaly in the center (dark gray) is due to steam, high velocity anomalies on the flanks (white) are due to the high-pressure front. interp-vp2 [ER]

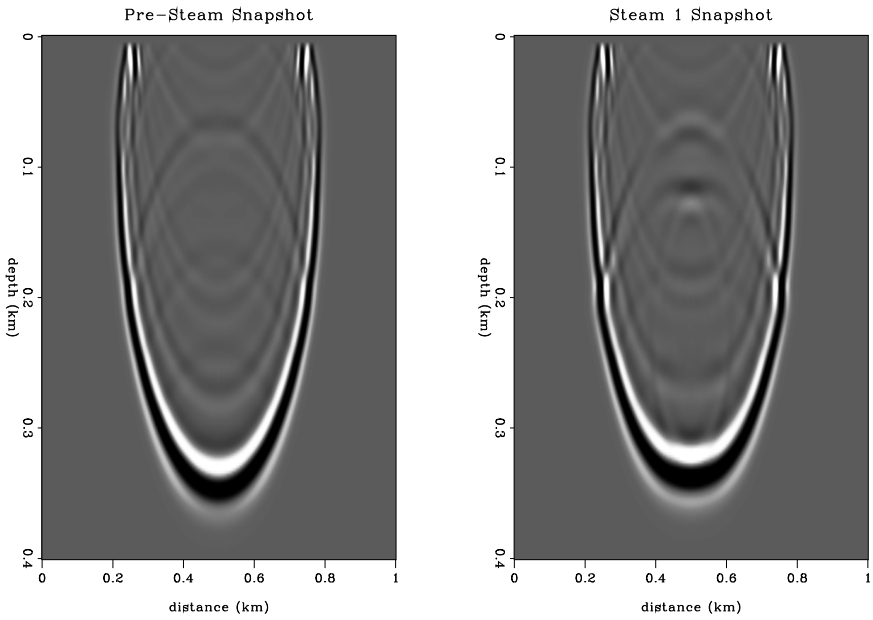

Figure 1.17: FD acoustic modeling wavefield snapshots: before steam injection (left), during steam (right). interp-waves12 [ER]

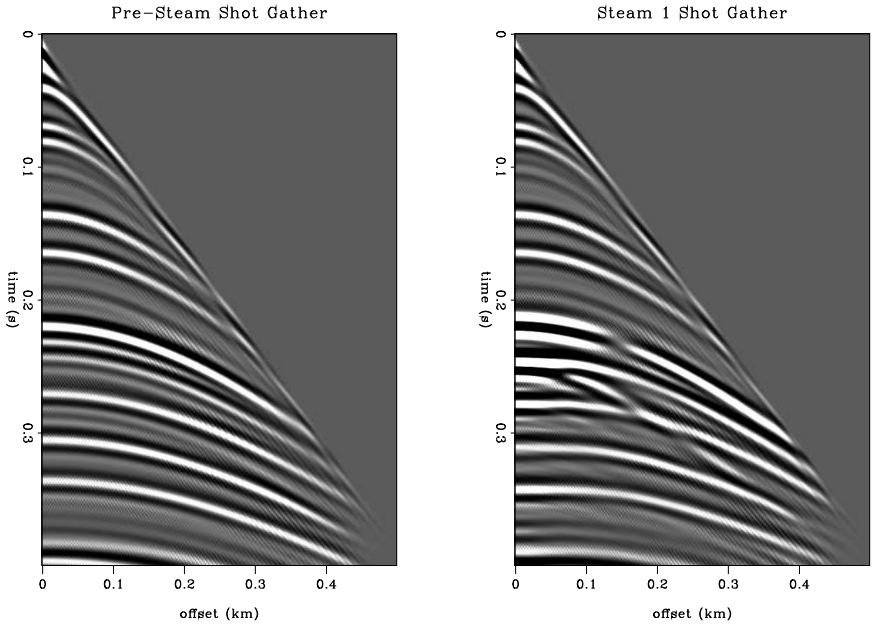

Figure 1.18: FD acoustic modeled shot gathers: before steam injection (left), during steam (right). interp-shot12 [ER]

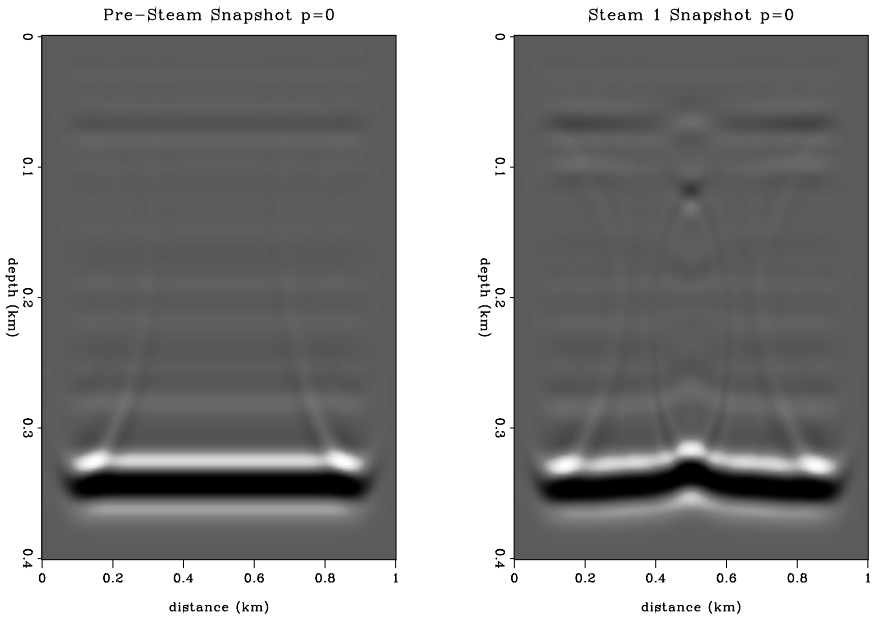

Figure 1.19: FD acoustic plane-wave snapshots: before steam injection (left), during steam (right). interp-pwave12 [ER]

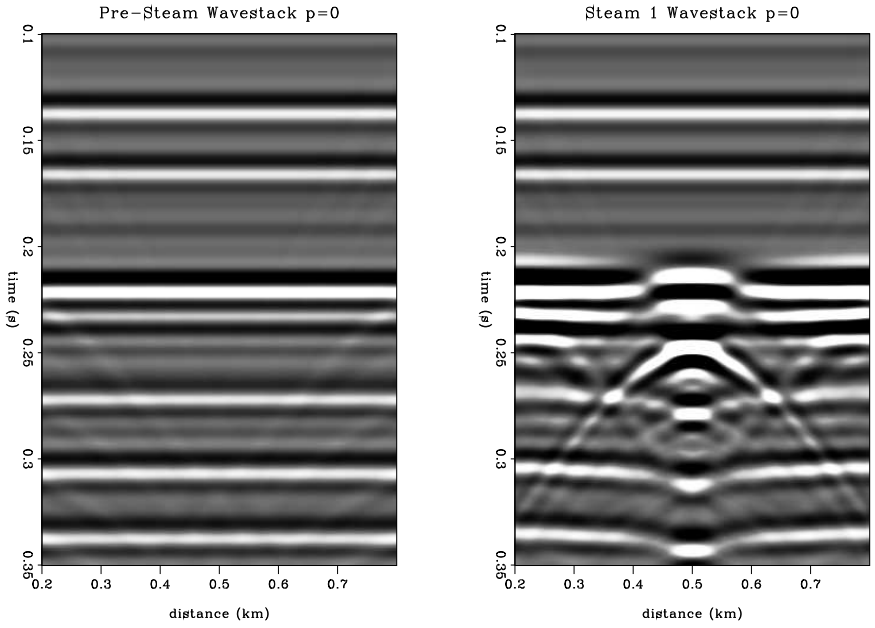

Figure 1.20: FD acoustic plane-wave wavestacks: before steam injection (left), during steam (right). interp-wstk12 [ER]

1.9 Traveltime and velocity analysis

At this point, I have discussed several seismic features visible in the time-lapse images and suggested correlations to the presence of steam, hot water and a high-pressure front. Furthermore, I have postulated an idealized steamflood fluid-flow model, and combined the basic physics of that model with rock physics lab measurements made on cores taken from the Duri site. This process gave rise to predictions that the steam zone should be seismically visible due to velocity decreases of 40%, large time delays, and strong impedance contrasts (reflections and diffractions). The hot water zone should show a 10% increase in velocity, while the hot oil zone should be seismically transparent. The high-pressure front should be visible from 20% velocity increases causing large time pull-ups and possible reflectivity changes along boundary layers. The seismogram modeling section demonstrated all of these predicted seismic responses qualitatively from a simple steamflood velocity model based on the core data and the idealized steamflood physics.

In this section, I present a detailed traveltime and velocity analysis of the reservoir zone to estimate traveltime and velocity changes directly from the six time-lapse data sets. Because this is a time consuming effort, I concentrate only on the east-west inline section that connects the steam injector with the two temperature monitor wells of Figure 1.1.

1.9.1 Traveltime picks

I made traveltime picks along the base of the P formation where earlier discussion suggested that the steam changes would be the largest. The traveltime picks are overlain on each inline section in Figures 1.21 to 1.26. On the east side of the well the picks are a little difficult to make because of the polarity reversal along the base of the reservoir reflection. To better visualize which event to pick, I made an animated series of frames showing the sections in chronological order. That greatly aided the interpretation of which reflector was moving where.

1.9.2 Traveltime curves

The traveltime picks for all six surveys are displayed together as traveltime curves in Figure 1.27. Each curve is labeled with its number in the series of time-lapse surveys. For example, label "2" means the picked curve from the second monitor survey, after 5 months of steam injection. It is evident from these curves that there is a lot of time delay in the center at the steam injector, and the time delay increases with calendar time. Also notable is the fact that the first three monitors show a time pull-up to the west of the injector, which would correspond to a pressure front. Directly to the east of the injector, a small time pull-up might be indicative of a hot water ring of condensed steam. Farther to the east, relatively small time changes are evident, suggesting the reservoir is at ambient conditions there.

1.9.3 Traveltime changes

Figure 1.28 shows the traveltime changes along the base of the reservoir, obtained by subtracting each traveltime curve from the baseline traveltime curve. In the center at the steam injector, traveltime delays occur. The first three monitor surveys show traveltime delays of about 10 ms, and the fourth and fifth monitors show increasing traveltime delay at about 15 and 20 ms respectively. This indicates that the steam zone is expanding and heating adjacent rock. To the west of the injector, traveltime pull-ups of about 10–15 ms occur during the first three monitors. This is consistent with a pressure front propagating to the west. At monitor surveys 4 and 5, the traveltime change decreases somewhat, probably due to a thermal front moving out radially and decreasing the velocity. To the east the traveltime changes are small, indicating that not much fluid flow is occurring in that direction.

1.9.4 Velocity analysis

Traveltime changes can be approximately converted to velocity changes with the following simple expression:

$$\Delta v \approx -v\frac{\Delta t}{t_r}\,, \tag{1.1}$$

where Δv is the change in velocity in the reservoir, v is the background rms velocity before steam injection, Δt is the time delay measured between two time-lapse surveys, as plotted in Figure 1.28, and t_r is the two-way interval traveltime through the reservoir using the background velocity.

For the Duri reservoir, I assumed an rms velocity value of 1.75 km/s, and a reservoir interval transit time of 50 ms. I used these valued with (1.1) and the curves of Figure 1.28 to compute changes in velocity in the reservoir for each time-lapse survey. The velocity changes are computed as an average vertical value within the reservoir.

1.9.5 Velocity contrasts

Figure 1.29 shows the resulting changes in velocity. In the center of the pattern, at the steam injector, the velocity decreases by up to 800 m/s after 19 months of steam injection. Assuming an interval velocity of 2.0 km/s for the reservoir, this velocity contrast works out to be -40%, which is exactly what was predicted by the steamflood model and core data! To the west of the injector, the velocity initially increases by about 400 m/s, which is about +20%. Again, this is exactly what was predicted for the pressure front in the absence of heat. At 13 and 19 months (monitors 4 and 5), the pressure front loses some of its velocity contrast, probably due to heating from the expanding steam zone. On the east side, a 100–200 m/s velocity increase (+5–10%) is consistent with an annulus of hot water. Beyond that, the reservoir changes

very little until the fifth survey where a velocity decrease of 200 m/s (-10%) seems to indicate heat has just arrived.

Figure 1.21: Traveltime picks before steam injection interp-res0t [ER]

Figure 1.22: Traveltime picks after 2 months of steam interp-res1t [ER]

Figure 1.23: Traveltime picks after 5 months of steam interp-res2t [ER]

1.10 Integrated interpretation

In this section, I interpret the combined analysis of the steamflood model, rock physics, seismic modeling, and field data observations. I have plotted the computed velocity contrasts as 2-D models to see the spatial effect of the propagating velocity changes (Figures 1.30 to 1.34). I have plotted 3-D migration profile images from all six surveys at the same inline location which passes through the injection well and the two temperature observation wells (Figures 1.35 and 1.36). Additionally, migrated time slices near the base of the P formation are plotted in Figures 1.37 to 1.41. The temperature observation well data are plotted in Figure 1.42.

1.10.1 At 2 months

At 2 months, the steam zone is already visible, and shows up as a 10–15% decrease in velocity, and bright diffractions and reflections at the injector location (Figures 1.30 and 1.35). Because the velocity decrease is not maximal compared to core measurement predictions for steamed rock, steam saturation may only be about 25% on average vertically. The width of the steam zone appears to be about 50 m, and is fairly radial as shown in Figure 1.37. A steam leak is apparently visible from the time delays in the overburden at about 75 ms pseudodepth.

To the north and west of the injector, a transient pressure front propagates away from the injection well. It is marked by a 20% increase in P-wave velocity, which matches predictions made by the steamflood model and the Duri core data. To the immediate west of the injector, a small increase of 10% in P-wave velocity may correlate with a ring of hot water (condensed steam), which is seen to form an annulus in the time slice of Figure 1.37. Beyond that, to the east, relatively little change in velocity has occurred. However, a polarity reversal is developing along the base of the P formation reflector, which may indicate that gas saturation increases are changing the seismic impedance within the reservoir, with little effect on the velocity; or that heating in the K formation below the main reservoir is changing the impedance

Figure 1.24: Traveltime picks after 9 months of steam interp-res3t [ER]

Figure 1.25: Traveltime picks after 13 months of steam interp-res4t [ER]

contrast at the P/K boundary. These results suggest that heat from the injector has not arrived at either of the temperature observation wells at this time, which correlates with the well data of Figure 1.42.

1.10.2 At 5 months

The velocity model of Figure 1.31 shows that the steam zone has expanded outwards to a width of perhaps 60 m. Heating and steam saturation has increased near the injector since the velocity has decreased an additional 5% since the last monitor. This heating appears to have propagated about 25 m outward to the west, and less to the east. The pressure front is still intact, and the polarity reversal along the base of the P formation seems complete (Figure 1.35). Reflections from the steam zones at the top of the P formation, bottom, and K formation appear stronger than at 2 months, indicating higher steam saturation values. The time slice of Figure 1.38 shows that the steam zone has remained about the same radial dimensions as at 2 months. The temperature monitor wells indicate that a small amount of heat has arrived to the west, but none to the east.

1.10.3 At 9 months

The velocity decrease at the injector has now increased to -20% on average in the interval. The pressure front appears to be intact. The steam zone seems not to have expanded outward much, but has intensified in place (Figure 1.32). The migrated profile and time slice of Figure 1.36 and 1.39 seem to support this conclusion since the steam reflections have increased in amplitude, but not much in diameter. The steam leak seems to have penetrated nearly down to the top of the P formation at this point, as visible in the migrated profile image. The temperature observation wells of Figure 1.42 show that the heating has increased to the west, but still nothing has arrived at the eastern observation well, which is supported by the seismic results.

1.10.4 At 13 months

Between 9 and 13 months, a major fluid-flow breakthrough has occurred to the north and west. The steam zone has expanded to the northwest as seen in the time slice of

Figure 1.26: Traveltime picks after 19 months of steam interp-res5t [ER]

Figure 1.27: Traveltime picks along the base of the P formation from all six time-lapse seismic images. interp-tcurves-ann [ER]

Figure 1.28: Traveltime changes along the base of the P formation from all six time-lapse seismic images. interp-dtcurves-ann [ER]

Figure 1.40. A thermal front has propagated to the west and probably to the north as seen by the velocity model of Figure 1.33. The pressure front has propagated almost entirely out of the seismic survey area to the west and probably north. Still relatively little is happening to the south and east of the injector.

The width of the steam zone at the base of the P formation is about 80 m at this time. A small steam zone is clearly imaged at the top of the P formation (165 ms) in Figure 1.36, and a larger steam zone is visible at the base of the P formation (200 ms). A weaker steam zone appears in the migrated image around 240 ms pseudodepth. The temperature logs of Figure 1.42 indicate that major heating has arrived to the west, but no heat has arrived yet to the east, which matches the time slice of Figure 1.40.

These results support the hypothesis that the pressure front may be an indicator of which direction future heat flow will preferentially propagate. Initially, the pressure front was observed to the northwest, but not the southeast. Now, the steam and thermal fronts seem to be following the lead of the pressure front and are moving to the northwest also, but not toward the southeast.

1.10.5 At 19 months

At 19 months, the steam zone has expanded even further outward towards the northwest as seen in the time slice of Figure 1.41. More heat has been transferred into the reservoir, as seen by the pronounced velocity decreases to the east and west of the injector in Figure 1.34. The pressure front has propagated almost completely out of the survey area, and is trailed by a strong thermal front toward the west. For the first time, a substantial velocity decrease is observed to the east in Figure 1.34. The suggestion from the seismic data that heat has now propagated in both the east and west directions is supported by the temperature logs of Figure 1.42, in which the first heating at the eastern observation well T2 has been recorded.

The steam disk has a full -40% change in velocity, which suggests that the entire reservoir thickness is saturated with steam in a 100 m diameter disk centered on the injector. The temperature log for the T1 well on the west shows temperatures of over 300 °F(steam), which implies that the steam front has propagated a full 100 m from the injector to the west. The time slice of Figure 1.41 seems to show the edge of the

Figure 1.29: Velocity changes along the base of the P formation from all six time-lapse seismic images. interp-dvcurves-ann [ER]

steam front has just arrived at the T1 well, which is in nice agreement with the well data. Extrapolating this seismic and well tie, the time slice suggests that steam has propagated perhaps as far as 150 m or more to the northwest of the injector.

1.11 Conclusion

It appears that the bright reflection disk centered on the injector well and the time delay beneath must indicate the extent of the steam zone, not merely hot fluid. The rock physics analysis has shown that the steam zone should be expected to show velocity decreases of up to 40%, whereas hot water or oil increases velocity by only 10% or less. Finite difference modeling of a reasonable steamflood velocity model shows strong diffractions and bright reflections emanating from the steam zone, that can be interpreted to match similar features in the field data. This analysis implies that the steam zone is about 40 m in diameter at the top of the P reservoir, 80 m in diameter at the base of the P reservoir, and heading to the north and west much faster than the south and east. This correlates with core measurements that the top part of the reservoir is at least one order of magnitude less permeable than the bottom part, and that for at least 13 months of steam injection, substantial heating had arrived at the T1 temperature monitor well to the west, but not the T2 well to the east.

My analysis suggests that the hot oil ring may be seismically transparent, but that the hot water ring might be visible since it causes about a 10% velocity increase. Close inspection of the time slices in Figures 1.37 to 1.41 shows a thin dark gray ring surrounding the white steam disk. This ring is about 15 m thick and corresponds to time pull-up (velocity increase) in the migrated profile sections. The dark gray amplitude suggests it is of opposite reflection polarity to the steam zone, which matches the predicted hot water properties. This dark gray ring may be the seismic view of the hot water steam condensate.

I have predicted that a large area of the 7-spot pattern would be subject to a fast-propagating cold high-pressure front. This pressure front should be seismically visible since it causes a 20% increase in velocity. Finite difference modeling shows that the high-pressure front can cause time pull-ups on seismic events due to velocity increase. The velocity models of Figures 1.30 to 1.34 show that the pressure front is propagating to the west, but not the east. Correlating the pull-up to features in the time slices of Figures 1.37 to 1.41 suggests that the pressure front propagates both north and west, but not south or east. Since the steam front is also observed to propagate to the northwest, but not the southeast, after 1 year of steam injection, it appears that mapping the early pressure front movement can be used to predict subsequent thermal and steam front fluid-flow propagation directions, many months in advance. This may be the most important result of my analysis of the Duri 4-D seismic monitoring data set.

Figure 1.30: Reservoir velocity at 2 months interp-vres1-ann [ER]

Figure 1.31: Reservoir velocity at 5 months interp-vres2-ann [ER]

Figure 1.32: Reservoir velocity at 9 months interp-vres3-ann [ER]

Figure 1.33: Reservoir velocity at 13 months interp-vres4-ann [ER]

Figure 1.34: Reservoir velocity at 19 months interp-vres5-ann [ER]

Figure 1.35: 3-D migrated inlines from the first three 3-D surveys. Baseline survey (left), first monitor after steam injection (center), and second monitor survey (right). interp-mig05a-ann [ER]

Figure 1.36: 3-D migrated inlines from the last three 3-D surveys. Third monitor survey after steam injection (left), fourth monitor (center), and fifth monitor survey (right). interp-mig05b-ann [ER]

Figure 1.37: 3-D migrated time slice at the base of the reservoir after 2 months of steam injection. T1 and T2 are the temperature observation well positions. interp-m1-tslice-ann [ER]

Figure 1.38: 3-D migrated time slice at the base of the reservoir after 5 months of steam injection. T1 and T2 are the temperature observation well positions. interp-m2-tslice-ann [ER]

Figure 1.39: 3-D migrated time slice at the base of the reservoir after 9 months of steam injection. T1 and T2 are the temperature observation well positions. interp-m3-tslice-ann [ER]

Figure 1.40: 3-D migrated time slice at the base of the reservoir after 13 months of steam injection. T1 and T2 are the temperature observation well positions. interp-m4-tslice-ann [ER]

Figure 1.41: 3-D migrated time slice at the base of the reservoir after 19 months of steam injection. T1 and T2 are the temperature observation well positions. interp-m5-tslice-ann [ER]

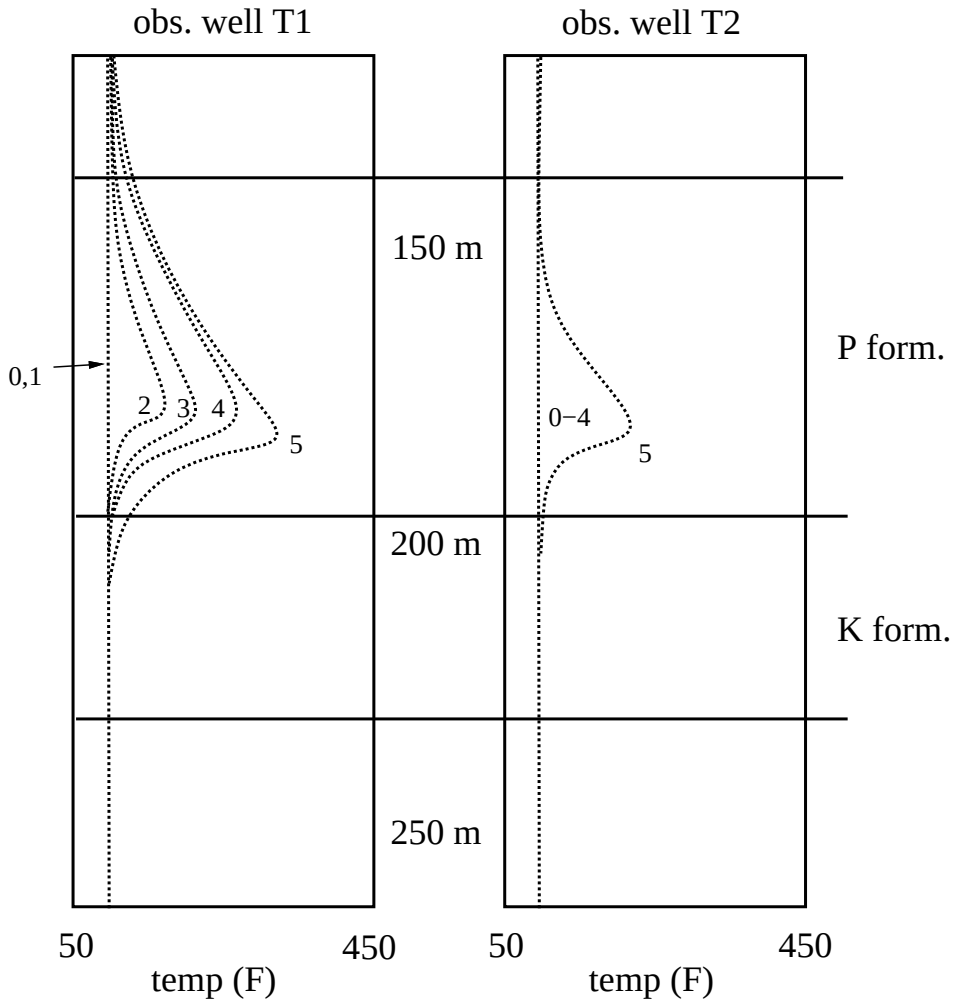

Figure 1.42: Temperature observation well data to the west (T1) and east (T2) of the steam injector. interp-temp [NR]

1.12 Future work

Much work remains to be done with this complex and fascinating data set. A top priority would be to map the data volumes properly in depth so that depth slice images can be interpreted accurately. Unfortunately, since lateral velocity variations within the reservoir are very strong, expensive depth migration methods are needed to perform this task. And 3-D depth migration, in turn, requires an accurate estimate of the 3-D subsurface interval velocity model.

Aside from imaging work, it would be very interesting to collaborate with someone on doing fluid-flow simulations of the steamflood process. These results could then be mapped through rock physics transformations with the core measurements to seismic properties. Then full waveform seismic modeling could be done and the result could be compared with the field data.

Taking that train of though one step further brings us to the ultimate – "seismic history matching". One could imagine constructing a complete iterative loop of fluid-flow simulation, rock physics transformation, seismic modeling, history matching with production data and seismic time-lapse data, and updating the reservoir simulation model. This integrated modeling and processing sequence offers exciting new possibilities for the future of optimal hydrocarbon reservoir management and controlled fluid-flow processes.

1.13 Acknowledgments

The seismic monitor data were kindly provided by Steve Jenkins (CalTex), Fred Herkenhoff and Ray Ergas (Chevron). Zhijing Wang (Chevron) provided the Duri core measurement information. Steve Jenkins provided many useful comments regarding the 4-D interpretation.

ZONE	P (psia)	ΔP (psia)	T (F)	ΔT (F)	Sg (%)	ΔSg (%)
steam	250	+150	350	+250	90	+80
hot water	200	+100	250	+150	0	-10
hot oil	175	+75	175	+75	0	-10
pressure front	150	+50	100	+0	0	-10
ambient	100	—	100	—	10	—

Table 1.2: Pressure, temperature and saturation changes in the steamflood model.

ZONE	ΔV_p	$\Delta\rho$
steam	-40%	-15%
hot water	+10%	0%
hot oil	0%	0%
pressure front	+20%	0%

Table 1.3: Predicted velocity and density changes in the steamflood zones.